Positron states and annihilation characteristics at the (100), (110), and (111) surfaces of alkali metals

N. G. Fazleev,* J. L. Fry, and A. H. Weiss
Department of Physics, The University of Texas at Arlington, Box 19059, Arlington, Texas 76019-0059
(Received 12 January 1998)

In this paper we present results of theoretical studies of positron states and annihilation characteristics at the clean surfaces of alkali metals. Positron surface states and positron work functions have been computed for the (100), (110), and (111) surfaces of Li, Na, K, Rb, and Cs using the modified superimposed-atom method to account for discrete-lattice effects, and the results are compared with those obtained for the transition-metal surfaces. Stable positron surface states are found in all cases, with the Li states lying about 0.5 eV below the bulk positron band, and other alkali metals having positron surface states a few hundredths of an eV below the bulk bands. The results for the positronium activation energy and positronium work function for the clean surfaces of alkali metals are presented as well. Surface and bulk state lifetimes and probabilities for a positron trapped in a surface state to annihilate with relevant core-level electrons are also computed and compared with available experimental data. [S0163-1829(98)06819-2]

I. INTRODUCTION

The long-range interaction of a charged particle with a semi-infinite medium (the attractive image potential) may in some cases lead to a bound state localized in the region of the vacuum-medium interface. Examples are provided by electrons trapped at surfaces of atomic and molecular (nonpolar) insulators, such as He, Ne, H_2, and D_2,[1] and by electrons trapped at the surface of an ionic crystal, such as LiF, by surface polarons.[2] These states should be distinguished from electron surface states, which are associated with energy gaps in the bulk band structure and are due to the termination of the three-dimensional periodicity. For positrons, the image-potential-induced surface states were first proposed by Hodges and Stott to explain the anomalous characteristics of positron annihilation observed in irradiated materials containing voids.[3] Using the attractive image potential on the vacuum side, and a constant potential equal to $-\Phi_p$ on the bulk side, where Φ_p is the positron work function (i.e., the positron ground-state energy in the bulk with respect to the vacuum level), and eliminating the divergence of the image potential near the surface by imposing a cutoff at -6.8 eV (the positronium binding energy), they predicted the existence of positron surface states on a number of metals.

Nieminen and Hodges[4] estimated the dynamic corrections to the image potential of a charged particle at a metal-vacuum interface variationally. Describing the electron-positron interaction in terms of virtual excitations of surface and bulk plasmons and employing a pseudopotential that mimics the effects of the electrostatic surface dipole and the repulsion from the ionic cores in the metal, they calculated the binding energy E_b of bound positron states on metal surfaces. Those studies[4] confirmed that for some metals the positron surface state is the ground state of the system consisting of a semi-infinite metal and a positron. Improved variational estimates of E_b and positron surface-state lifetimes were later obtained in Refs. 5–7. Positron states on metal surfaces were also studied within an atomistic model of Nieminen and Puska,[8–10] which included discrete-lattice effects. Other theoretical studies of positron states on metal surfaces were performed within a nonlocal theory,[11] a hydrodynamic model,[12] and within a physisorbed positronium picture for the positron surface state.[13] Direct experimental evidence for the existence of positron surface-bound states on metals has been provided by the observation that at elevated temperatures positrons could be thermally desorbed from surfaces of these metals into the vacuum as positronium.[14–17]

Recently the nature and location of positron bound states at metal surfaces, both clean and adsorbate-covered, have become the subject of experimental studies using positron-annihilation-induced Auger-electron spectroscopy (PAES).[18–25] In PAES experiments most of the low-energy positrons, implanted into the sample under study, diffuse back to the vacuum-solid interface where on the order of half are trapped into a surface state.[18,25] A certain fraction of the surface trapped positrons annihilates with neighboring core-level electrons, creating core-hole excitations that give rise to Auger-electron emission.[18,25] Since the positron-annihilation-induced Auger-electron intensities are sensitive to the spatial distribution of the positron wave function on the surfaces of interest, this new technique provides an experimental tool to make site-sensitive studies of the positron annihilation process.[10,19,20,26–29] These experiments have stimulated this theoretical work for alkali metals.

The existence of positron states at the surfaces of alkali metals was examined previously by Nieminen and Hodges, who performed calculations describing a metal in the jellium approximation and electron-positron correlations within the framework of the plasmon model.[4] Although positron surface bound states on alkali metals were predicted, they found the positron ground-state energy in the bulk to be lower than the energy of the positron surface state, thus concluding that positrons would not form stable surface bound states on alkali metals.

Discrete lattice effects were not considered in their work, and a consistent reference level of energy was not achieved

between bulk and surface states as a result of their treatment of the surface dipole layer contribution to the energies and their use of different computational schemes and potentials in estimates of E_b and Φ_p.

The purpose of the present paper is to perform first-principles calculations of positron surface states and positron work functions for the clean (100), (110), and (111) surfaces of alkali metals improving these two approximations, to determine whether or not alkali metals should be expected to support positron surface states, and to study positron annihilation characteristics at alkali-metal surfaces. Positron surface and bulk states are computed in this paper from the same potential within a modified superimposed-atom method, taking into account discrete-lattice effects. These calculations are the first such calculations to our knowledge for alkali metals. They are indispensable for clarifying the formation, stability, and localization of positron surface states, information needed for the interpretation of PAES studies.

Section II of this paper details the construction of a potential for a positron at the alkali-metal surface from the full three-dimensional electron density at the surface. Section III presents the results of calculations of positron surface bound states at the (100), (110), and (111) surfaces of Li, Na, K, Rb, and Cs by solving a single-particle Schrödinger equation numerically using a relaxation technique.[8,30] Localization of the positron at the alkali-metal surfaces is determined, and the positron binding energies in the surface states are computed as well. Section IV presents the results of calculations of the positron work function, positronium activation energy, and positronium work function for alkali metals. Positron annihilation characteristics are determined in Sec. V. Positron surface-state annihilation characteristics are compared with the ones computed for the bulk alkali and transition metals and for the clean (100), (110), and (111) surfaces of Cu. Discussion of the obtained results and possibilities of observation of the PAES signals from the alkali-metal surfaces is presented in Sec. VI. The conclusions drawn from this work are summarized in Sec. VII.

II. POSITRON POTENTIAL AT A METAL SURFACE

The calculations reported in this paper are performed using a modified superimposed-atom method in which the potential experienced by a positron at a metal surface is written as the sum of an electrostatic Hartree term, $V_H(\mathbf{r})$, and an electron-positron correlation term, $V_{\mathrm{corr}}(\mathbf{r})$:

$$V(\mathbf{r}) = V_H(\mathbf{r}) + V_{\mathrm{corr}}(\mathbf{r}). \tag{1}$$

The Hartree potential $V_H(\mathbf{r})$ is constructed as a superposition of the atomic Coulomb potentials $V_{\mathrm{Coul}}^{\mathrm{at}}(|\mathbf{r}-\mathbf{R}|)$ from all the atoms located within a predetermined radius of the evaluation point, where $\mathbf{R}$ defines the positions of the host nuclei. Atomic calculations are performed self-consistently within the local-spin-density approximation,[31] using the exchange-correlation functional and atomic configurations from Refs. 32 and 33, respectively. The superposition of free atomic charge densities gives a total three-dimensional charge density at the surface that decays exponentially into the vacuum, resulting in a surface dipole layer. A disadvantage of the superposition of free atomic charge densities is that the resulting dipole layers are consistently too large.[34] However, this effect can be compensated for by calculating the self-consistent atomic charge densities for an atom placed in a spherically symmetric ''stabilizing'' potential well.[34] The effect of the ''stabilizing'' well is the contraction of the charge densities, thereby providing a dipole layer that gives the proper electron work function for the surface constructed from the superimposed atoms. Accordingly, we modify the atomic electron density calculations by placing alkali-metal atoms in a ''compensating'' potential well of magnitude -0.25 Ry, extending from the atom center out to one Wigner-Seitz radius, then linearly ramping to a value of 0.00 Ry at twice the Wigner-Seitz radius and beyond. This potential well has been used for a large variety of metal surfaces and produces results for the electron work function in reasonable agreement with the experimental data.[34,35] Note, the result of using such a potential well is that it leaves the atomic-wave-function shape virtually unchanged within the Wigner-Seitz cell while modifying the exponentially decaying tail outside the cell.

The Schrödinger equation is then solved self-consistently for each bound electron state of each alkali-metal atom. The criterion for convergence is that the change in the energy of each bound electron from one iteration to the next is less than 10^{-8} Hartree. The resulting wave functions then provide the electron densities and corresponding atomic potentials via Poisson's equation. The crystal structure and the lattice constant for the bulk alkali metals are taken from Ref. 36. The resulting total electron density $n_-(\mathbf{r})$ at the alkali-metal surface is approximated by the superposition of the calculated contracted atomic electron densities:

$$n_-(\mathbf{r}) = \sum_{\mathbf{R}} n_-^{\mathrm{at}}(|\mathbf{r}-\mathbf{R}|), \tag{2}$$

where the $\mathbf{R}$ summation takes place over the positions of the host nuclei. The Hartree potential $V_H(\mathbf{r})$ is constructed in a similar way:

$$V_H(\mathbf{r}) = \sum_{\mathbf{R}} V_{\mathrm{Coul}}^{\mathrm{at}}(|\mathbf{r}-\mathbf{R}|). \tag{3}$$

In constructing $V_{\mathrm{corr}}(\mathbf{r})$ at a surface, we exploit the fact that the correlation component of the positron potential deep inside and far outside the metal surface is described well by the local-density approximation (LDA) and the image potential, respectively. We then divide the space into two regions, namely, the bulk and image potential regions, where the two models are applied. The border between these regions is chosen to pass through the crossover point of the bulk and image potentials, located immediately outside the surface. The correlation part, $V_{\mathrm{corr}}(\mathbf{r})$, of the positron potential in regions of high electron density (the bulk region), which in general depends not only on $\mathbf{r}$ but also on the total three-dimensional electron density, $n_-(\mathbf{r})$, can be calculated accurately using the LDA. In the LDA, V_{corr} is obtained assuming the positron at a given position to be embedded in a homogeneous system with an electron density being equal to the actual electron density at that particular point, i.e., $V_{\mathrm{corr}}^{\mathrm{LDA}}(\mathbf{r};n_-) = V_{\mathrm{corr}}^{h}(n_-(\mathbf{r}))$, where V_{corr}^{h} is the correlation energy of a positron in a homogeneous electron gas of density n_-.[37]

This approximation is justified by the fact that, inside a bulk metal, the positron wave function mainly resides in the interstitial regions between the atoms, where the electron density is slowly varying. The parametrization of Boronski and Nieminen[38] is used for the electron density dependence of $V_{\mathrm{corr}}(n_-(\mathbf{r}))$.

Outside the metal surface, we express the correlation part of the total positron potential as an image potential,

$$V_{\mathrm{image}}(\mathbf{r}) = -\frac{e^2}{4\pi\varepsilon_0}\frac{1}{4[Z_{\mathrm{eff}}(n_-(\mathbf{r}))-Z_0]}, \tag{4}$$

where e is the charge of the positron, ε_0 is the vacuum permittivity, $Z_{\mathrm{eff}}(n_-(\mathbf{r}))$ is the effective distance from the surface, represented as a function of the total electron density at the surface, $n_-(\mathbf{r})$, and Z_0 defines the effective image-plane position on the vacuum side of the top layer of atoms. Following the corrugated mirror model,[8–10,26,27] we construct the image potential that has the same corrugations as the total electron density, $n_-(\mathbf{r})$. The assumption is made that at large distances (low electron density) the corrugations in the image potential are negligible and Z_{eff} is equal to the coordinate perpendicular to the surface. Although outside the metal surface the actual form of the positron-metal interaction is complex and depends on the dynamical response of electrons to the positron motion, it has been shown that by an appropriate choice of the image surface, one can obtain a good description of the clean-surface properties using the image potential of Eq. (4) as an approximation to the dynamic and nonlocal image interaction.[8–10,26,27] The joining of the image potential to the local-density correlation potential is done by taking V_{corr} to be the smaller of the two at each point outside the surface.

III. POSITRON SURFACE STATES

The electron density and the positron potential are calculated in the node points of a three-dimensional mesh that forms the polyhedron capable by symmetry in the plane of the alkali-metal surface of describing the potential and wave functions. The positron is assumed to be in the ground state and delocalized in the plane of the alkali-metal surface, and to have a crystal momentum in this plane $\mathbf{k}=\mathbf{0}$. The outermost plane of the alkali-metal atoms is taken to reside at $Z=0$. The extent of the positron wave function into the vacuum outside the alkali-metal surface and inside the alkali-metal lattice is determined by the computational cell boundaries in the direction perpendicular to the surface (Z direction). These boundaries are chosen to be far (up to 10 lattice parameters) from the topmost layer of atoms. We solve a discretized version of the three-dimensional Schrödinger equation for the positron eigenenergy and for the positron wave function using a finite difference relaxation technique.[8,30] In particular, the value of the Laplace operator ∇^2 at a given point is written in terms of the values of the wave function at the six neighboring points. The positron wave function and the energy eigenvalue are found by solv-

TABLE I. Calculated values of positron surface-state binding energies, E_b, at the clean (100), (110), and (111) surfaces of Li, Na, K, Rb, Cs, Cu, and at the (100) surface of Cu and Ni covered with one physical monolayer of Cs. E_b (NH) denotes the results of Nieminen and Hodges (Ref. 4) for the positron surface-state binding energy. $E_b^{\mathrm{expt.}}$ denotes the experimental results for the positron surface-state binding energy (Ref. 14).

Metal	Lattice	r_s (a.u.)	Face	E_b (eV)	E_b (NH) (eV)	$E_b^{\mathrm{expt.}}$ (eV)
Cu	fcc	2.669	(100)	2.83	2.8	2.77(5)
			(110)	2.98	2.8	2.97(5)
			(111)	2.79	2.8	2.80(5)
Cu+Cs (1 ML)			(100)	4.37[a]		
Ni+Cs (1 ML)			(100)	5.00[b]		
Li	bcc	3.247	(100)	3.93	2.7	
			(110)	3.83	2.7	
			(111)	3.97	2.7	
Na	bcc	3.933	(100)	5.90	2.7	
			(110)	5.91	2.7	
			(111)	5.90	2.7	
K	bcc	4.863	(100)	4.83	2.6	
			(110)	4.86	2.6	
			(111)	4.85	2.6	
Rb	bcc	5.197	(100)	4.91	2.7	
			(110)	4.92	2.7	
			(111)	4.94	2.7	
Cs	bcc	5.626	(100)	4.92	2.9	
			(110)	4.98	2.9	
			(111)	4.95	2.9	

[a]Reference 27.
[b]Reference 9.

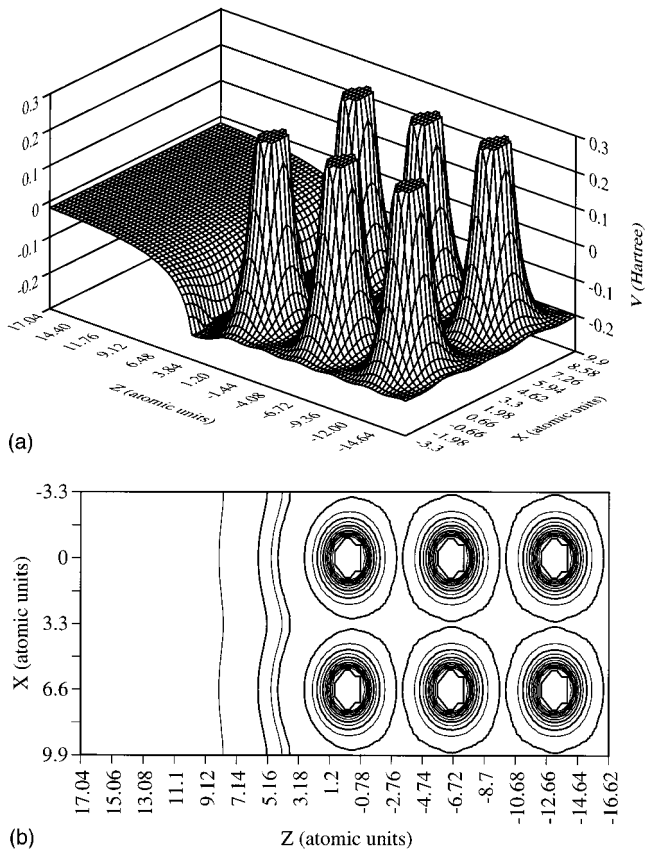

FIG. 1. Calculated potential for a positron trapped in a surface state at a clean (100) surface of Li. Panel *A* shows 3D plot for $Y=0$ (view from the bulk). Panel *B* shows contour plot in the X-Z plane for $Y=0$. Vacuum is at the left in panel *B*. Contours are separated by 0.05 hartree.

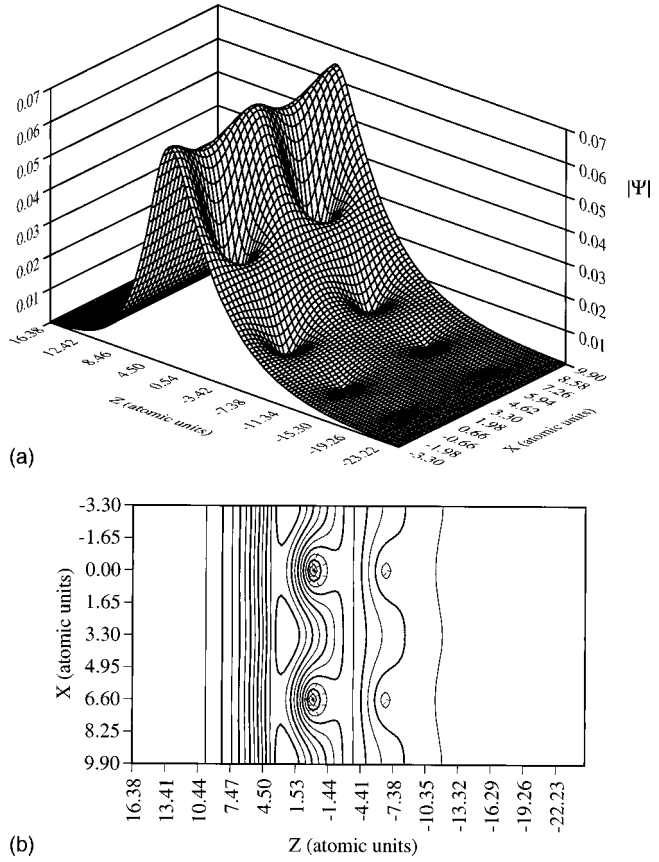

FIG. 2. Calculated ground-state wave function for a positron trapped in a surface state at a clean (100) surface of Li. Panel *A* shows 3D plot for $Y=0$ (view from the bulk). Panel *B* shows contour plot in the X-Z plane for $Y=0$. Vacuum is at the left in panel *B*. Contour spacings are 0.0025 atomic units.

ing iteratively for the energy, then correcting the wave function based on the energy, the potential, and the surrounding values of the wave function. In the numerical calculations the mesh density is doubled repeatedly until the calculated energy converges.

Delocalized states in the plane of the alkali-metal surface (the XY plane) are obtained by using boundary conditions that continue the wave function through the polyhedron surfaces (in the X and Y directions). The parameter Z_0 is chosen to be one Wigner-Seitz radius for bulk alkali metals from the plane of centers of the top layer of atoms along a reference line. This particular choice of the parameter Z_0 (one Wigner-Seitz radius for bulk metal) has reproduced the experimental binding energy of a positron trapped in a surface state at the clean (100) surface of Cu (Refs. 10 and 26–28) and has also reproduced the experimentally observed reduction of the Cu PAES intensity from the (100) surface of Cu covered with one physical monolayer of Cs compared to the clean surface case.[19,20,26–28] The Wigner-Seitz radii for the bulk alkali metals used in calculations are taken from Ref. 36.

The estimates of the positron surface-state binding energies, E_b, at the clean (100), (110), and (111) surfaces of Li, Na, K, Rb, Cs, and Cu are displayed in Table I. It follows from Table I that the computed values of the positron surface-state binding energies for Cu(100), Cu(110), and Cu(111) (E_b is equal to 2.83, 2.98, and 2.79 eV, respectively) agree quite well with the experimental positron surface-state binding energies [$E_b^{\text{expt.}}$ is equal to 2.77(5), 2.97(5), and 2.80(5) eV for Cu(100), Cu(110), and Cu(111), respectively] providing confidence in the theoretical procedures employed in calculations of E_b for alkali-metal surfaces.

A. Positron surface states at the (100), (110), and (111) surfaces of Li

Plots of the positron potential and positron surface bound wave function at the (100), (110), and (111) surfaces of Li are presented in Figs. 1–6. The following may be seen from these plots.

(a) The positron potentials for the clean (100), (110), and (111) surfaces of Li contain small corrugations that exist mostly on the vacuum side of the alkali-metal surface, as in the cases of the clean and covered with one physical monolayer of Cs adsorbate (100) surface of Cu.[26,27]

(b) Similar to the case of transition-metal surfaces, the positron is localized mainly in the image-correlation well on the vacuum side of the topmost layer of atoms. The positron surface-state wave functions at the (100), (110), and (111) surfaces have their maximum about 2.27, 2.09, and 1.90 a.u. outside the topmost layer of Li atoms into the vacuum, respectively, and they all experience a rapid drop with distance into the Li lattice as in the case of the clean transition-metal surfaces.[9,10,27] Slight differences in the position of the maxi-

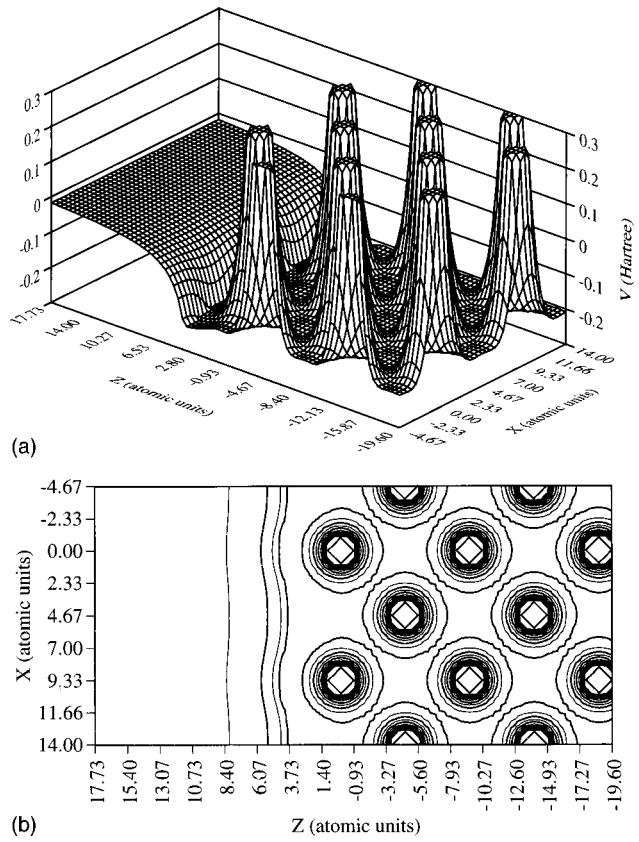

FIG. 3. Calculated potential for a positron trapped in a surface state at a clean (110) surface of Li. Panel *A* shows 3D plot for $Y=0$ (view from the bulk). Panel *B* shows contour plot in the X-Z plane for $Y=0$. Vacuum is at the left in panel *B*. Contours are separated by 0.05 hartree.

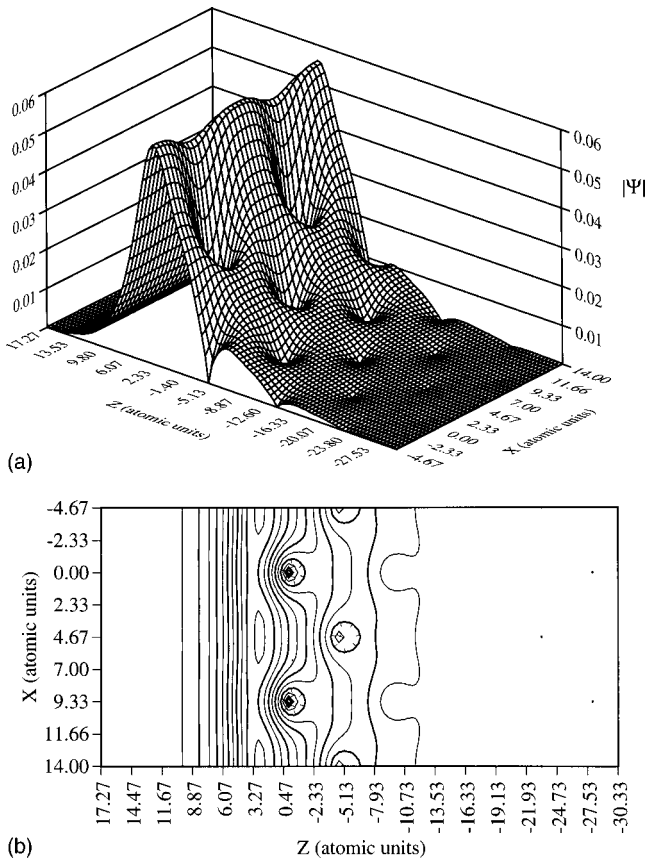

FIG. 4. Calculated ground-state wave function for a positron trapped in a surface state at a clean (110) surface of Li. Panel *A* shows 3D plot for $Y=0$ (view from the bulk). Panel *B* shows contour plot in the X-Z plane for $Y=0$. Vacuum is at the left in panel *B*. Contour spacings are 0.0025 atomic units.

mum of the positron surface-state wave functions at the (100), (110), and (111) surfaces and in the extent to which the wave functions penetrate into the Li lattice are due to differences in the atomic density of these surfaces.

Orientation-dependent variations of the atomic density and total electron density result in a corresponding dependence of the positron surface-state binding energy, E_b. The computed values of E_b for the (100), (110), and (111) surfaces of Li converge to 3.93, 3.83, and 3.97 eV with respect to the vacuum, respectively, and, thus, they exceed by about 1 eV the values for E_b found by the same procedure for the corresponding surfaces of Cu: 2.83, 2.98, and 2.79 eV, respectively. It also may be seen from Table I that, similar to the case of transition-metal surfaces, the largest values of E_b are correlated with the planes of smallest atomic density. The larger value of E_b for positrons trapped at the clean (100), (110), and (111) surfaces of Li as compared to E_b for the corresponding surfaces of Cu is due primarily to the increased depth of the correlation well for Li. The deeper well is a result in part of the lower total electron density in the alkali metal as compared to the transition metal, and to a change in the position of the image surface.

B. Positron surface states at the (100), (110), and (111) surfaces of the other alkali metals

Plots of the computed positron potential and positron surface-state wave function at the (100), (110), and (111) surfaces of other alkali metals (Na, K, Rb, and Cs) look similar to each other. Figs. 7–12 show the positron potential and positron surface-state wave function at the (100), (110), and (111) surfaces of Rb. The following may be seen from these plots.

(a) The positron potential at the clean (100), (110), and (111) surfaces of Na, K, Rb, and Cs contains small corrugations that exist mostly on the vacuum side of the alkali-metal surface and does not extend into the alkali-metal lattice. This is similar to the cases of the (100), (110), and (111) surfaces of Li and the transition-metal surfaces, both clean and covered with one physical monolayer of the alkali-metal adsorbate.[26,27]

(b) Instead of being localized mainly on the vacuum side of the topmost layer of atoms, as in the case of transition-metal surfaces and the clean (100), (110), and (111) surfaces of Li, the positron surface-state wave functions for Na, K, Rb, and Cs are found to extend up to several atomic layers into the alkali-metal lattice, having their maximum in the interstitial region between the topmost and the second layers of alkali-metal atoms. These wave functions, in general, drop off with distance into the lattice less rapidly than the positron surface-state wave functions at transition-metal surfaces. Slight differences in the extent to which the positron surface-state wave functions at the (100), (110), and (111) surfaces penetrate into the alkali-metal lattice are due to differences in the atomic density of these surfaces.

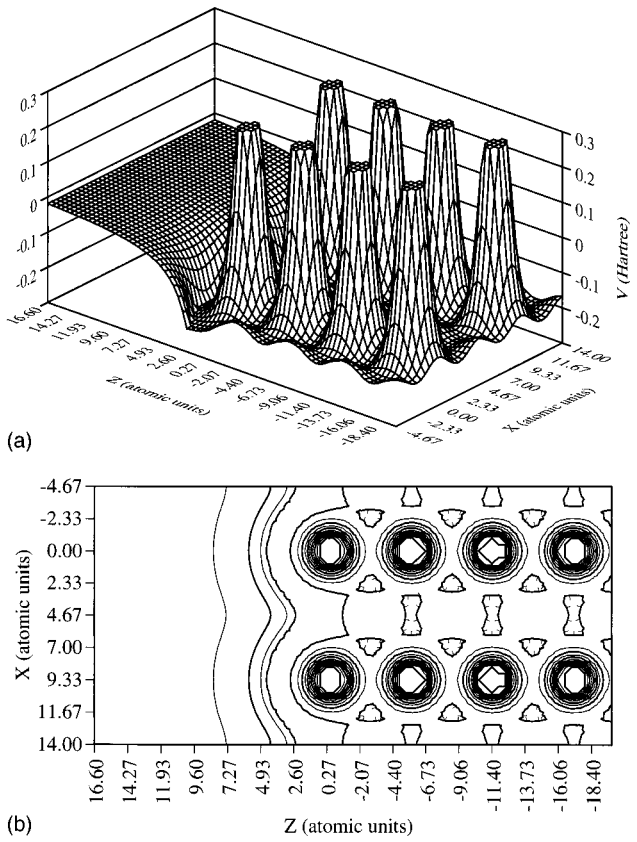

FIG. 5. Calculated potential for a positron trapped in a surface state at a clean (111) surface of Li. Panel *A* shows 3D plot for $Y=0$ (view from the bulk). Panel *B* shows contour plot in the X-Z plane for $Y=0$. Vacuum is at the left in panel *B*. Contours are separated by 0.05 hartree.

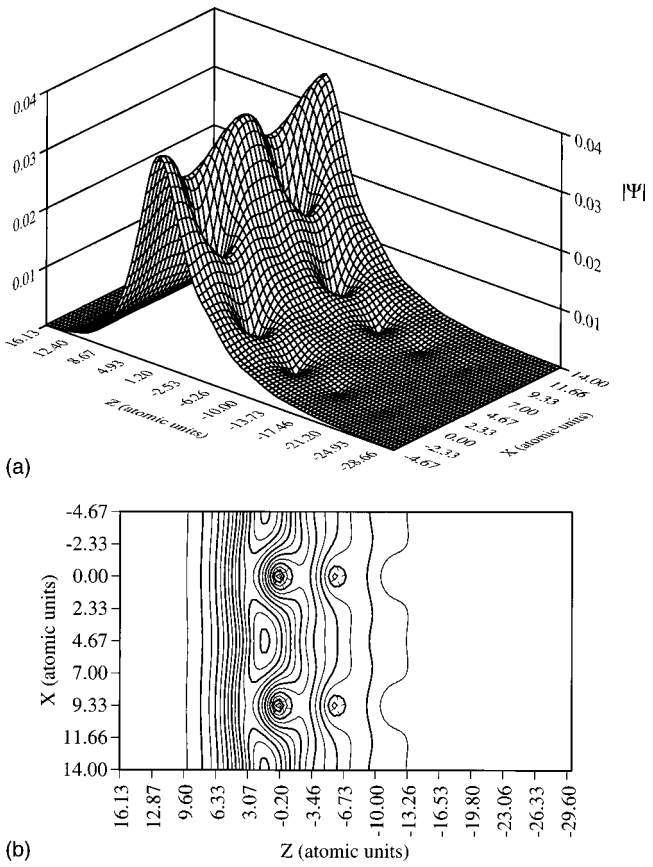

FIG. 6. Calculated ground-state wave function for a positron trapped in a surface state at a clean (111) surface of Li. Panel *A* shows 3D plot for $Y=0$ (view from the bulk). Panel *B* shows contour plot in the X-Z plane for $Y=0$. Vacuum is at the left in panel *B*. Contour spacings are 0.0025 atomic units.

It may be seen from Table I that the computed surface-state binding energies, E_b, measured with respect to the vacuum zero, for positrons trapped at the clean (100), (110), and (111) surfaces of Na, K, Rb, and Cs significantly exceed their values for positrons trapped at the corresponding surfaces of Cu (by about 3 eV for Na, and by about 2 eV for K, Rb, and Cs). On the other hand, the computed binding energies for positrons trapped at the clean surfaces of Na, K, Rb, and Cs are comparable with the ones obtained for positrons trapped at the (100) surface of Cu and Ni covered with one physical monolayer of Cs: $E_b=4.37$ and 5.00 eV, respectively.[9,26,27] As in the case of Li, the larger values of E_b for positrons trapped at the clean (100), (110), and (111) surfaces of Na, K, Rb, and Cs as compared to E_b for the corresponding clean surfaces of Cu reflect the increased depth of the correlation well for alkali metals. The deeper well at the alkali metal's surface is due in part to the fact that the position of the image surface has to be moved farther away from the outermost plane of alkali-metal atoms compared to transition-metal surfaces (the Wigner-Seitz radius for alkali metals is larger than the one for transition metals). Similar to the case of Cu, the binding energy of positrons trapped at the surfaces of Na, K, Rb, and Cs show a tendency that E_b is the largest for the surface of smallest atomic density. It also follows from Table I that estimates of the positron surface-state binding energies for alkali metals obtained in this paper differ significantly from the values obtained by Nieminen and Hodges.[4] These differences are attributed to a more accurate representation of the positron potential in the present paper and to discrete lattice effects that were not considered by those authors.

IV. POSITRON WORK FUNCTION

To predict the stability of the positron surface bound states at the alkali-metal surfaces, first-principles calculations of the positron work function, Φ_p (i.e., the ground-state energy in the bulk with respect to the vacuum zero level) are performed for Cu and for all studied alkali metals. To have a consistent reference level of energy, calculations of the positron ground-state energy in the bulk are performed with respect to the vacuum zero level, the same reference level of energy used in calculations of the positron surface-state binding energies. To avoid inconsistencies introduced by the use of different computational schemes and different potentials in calculations of the bulk chemical potential, μ_p, and the electrostatic potential barrier D contributing to Φ_p ($\Phi_p=-D-\mu_p$) and E_b, calculations of the positron ground-state energies in the bulk are performed on the basis of the modified superimposed-atom method employing the same total electron density and the same potential felt by the positron [again given by Eq. (1)] that are used in positron surface-state calculations. The positron ground-state energies with respect to the vacuum zero level for the bulk Cu and

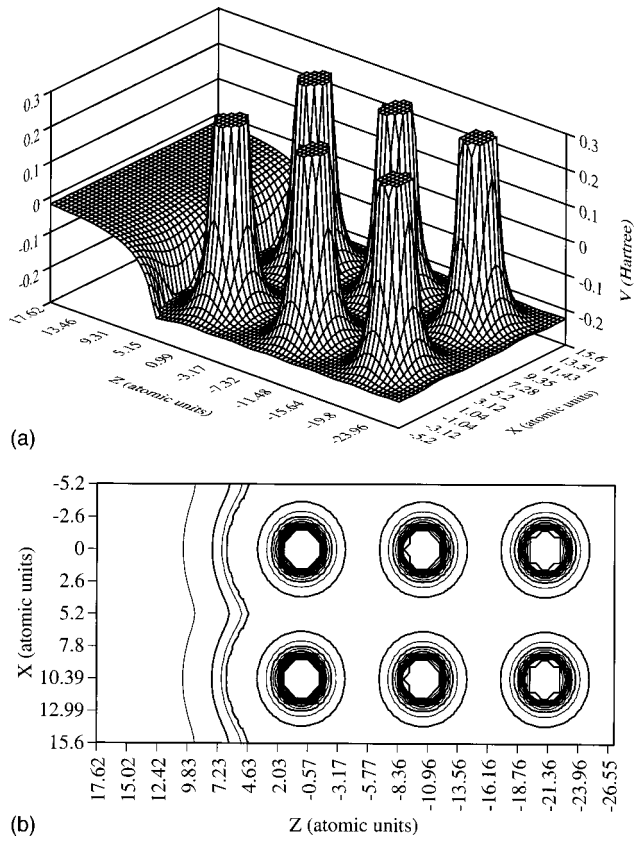

FIG. 7. Calculated potential for a positron trapped in a surface state at a clean (100) surface of Rb. Panel *A* shows 3D plot for $Y=0$ (view from the bulk). Panel *B* shows contour plot in the *X*-*Z* plane for $Y=0$. Vacuum is at the left in panel *B*. Contours are separated by 0.05 hartree.

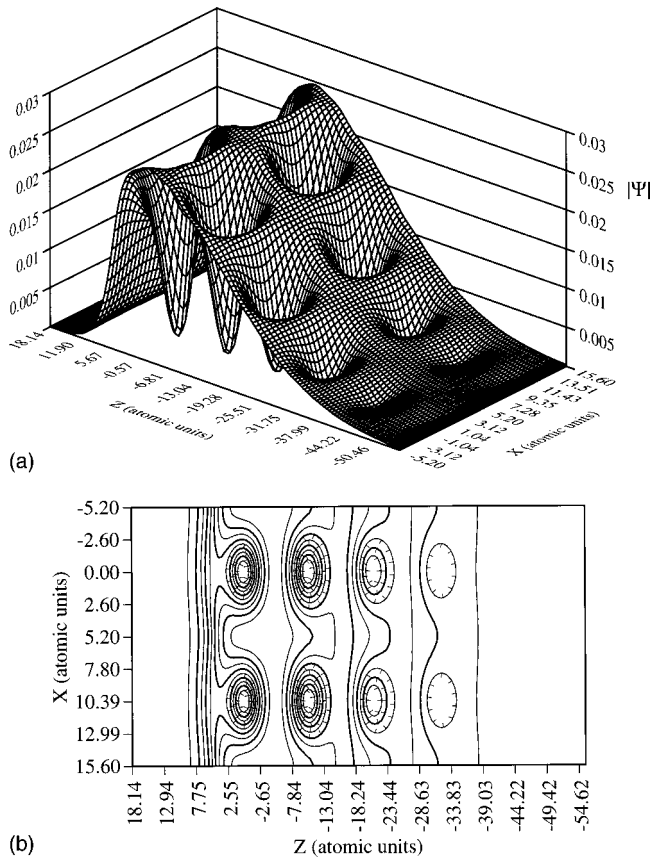

FIG. 8. Calculated ground-state wave function for a positron trapped in a surface state at a clean (100) surface of Rb. Panel *A* shows 3D plot for $Y=0$ (view from the bulk). Panel *B* shows contour plot in the *X*-*Z* plane for $Y=0$. Vacuum is at the left in panel *B*. Contour spacings are 0.0025 atomic units.

alkali metals are found by solving the three-dimensional Schrödinger equation numerically for a positron in the bulk metal terminated by the (100), (110), and (111) surfaces using the finite difference relaxation technique. Similar to positron surface-state calculations, the electron density and the positron potential are calculated in the node points of a three-dimensional mesh that forms the polyhedron capable by symmetry in the plane of the alkali-metal surface of describing the positron potential and wave functions. The computational cell boundaries are chosen to be far (up to ten lattice parameters) from the topmost layer of atoms in the direction perpendicular to the surface (*Z* direction) into the vacuum outside the alkali-metal surface and inside the alkali-metal lattice. It is assumed that the positron wave function deep inside the alkali metal approaches periodicity in the *Z* direction with a period of one lattice parameter and that $\mathbf{k}=\mathbf{0}$ is the lowest Bloch state. The density of mesh points in these calculations is chosen to be similar to that used in the surface-state calculations. The results for the positron work function are displayed in Table II. It follows from Table II that the computed values of the positron work function for Cu(100), Cu(110), and Cu(111) (Φ_p is equal to -0.23, -0.14, and -0.36 eV, respectively) agree quite well with the experimental positron work functions [$\Phi_p^{\text{expt.}}$ is equal to $-0.3(2)$,[43] $-0.2(2)$,[43] and $-0.4(1)$ eV,[44] respectively] providing confidence in the theoretical procedures employed in calculations of Φ_p. Similar to the behavior of the electron work function, Φ_p varies remarkably little in going from one alkali metal to another; for instance, the positron work functions vary from 3.50 eV for Li(100) to 4.89 eV for Cs(100), whereas the electron density varies by a factor of 5 going from Li to Cs. As Table II shows, Φ_p varies from surface to surface due to the changes in the total electron charge density at different surfaces, and the planes of smallest atomic density tend to have the largest positron work functions.

It may be seen from Table II that estimates of Φ_p obtained in this paper differ for most of the alkali metals from the values obtained earlier using other computational schemes.[39–42] The difference is the largest in the case of bulk Li terminated by the (100), (110), and (111) surfaces [for which the computed positron ground-state energies with respect to the vacuum level lie much higher (about 1–3 eV) than previously found].[39–42] The differences found are partially due to the fact that, unlike the work reported here in which a consistent reference level of energy was used and the same potential was employed while calculating the dipole and bulk contributions to Φ_p, earlier calculations used different potentials and different reference levels of energy in estimating the bulk chemical potential, μ_p, and the electrostatic potential barrier *D* contributing to Φ_p.[39–42]

Since in each case the positron surface-state energies are lower than the ground-state energies in the bulk, it may be concluded that the calculated positron surface states are stable on the (100), (110), and (111) surfaces of Cu and

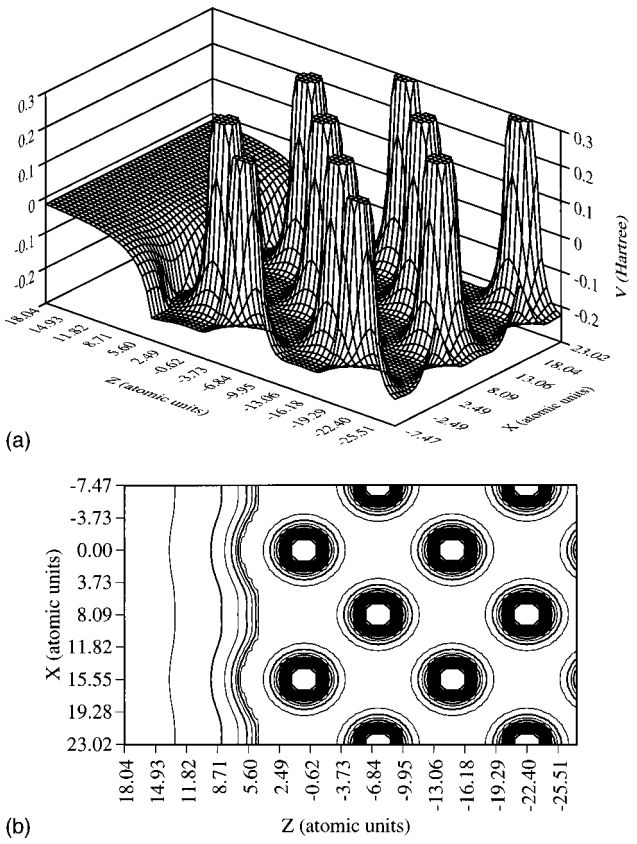

FIG. 9. Calculated potential for a positron trapped in a surface state at a clean (110) surface of Rb. Panel *A* shows 3D plot for $Y=0$ (view from the bulk). Panel *B* shows contour plot in the *X*-*Z* plane for $Y=0$. Vacuum is at the left in panel *B*. Contours are separated by 0.06 hartree.

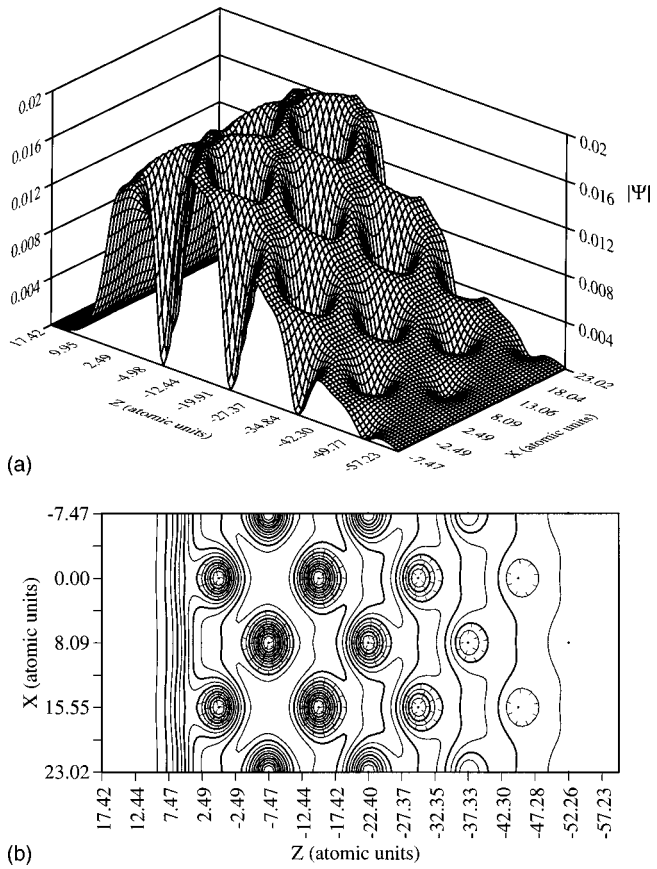

FIG. 10. Calculated ground-state wave function for a positron trapped in a surface state at a clean (110) surface of Rb. Panel *A* shows 3D plot for $Y=0$ (view from the bulk). Panel *B* shows contour plot in the *X*-*Z* plane for $Y=0$. Vacuum is at the left in panel *B*. Contour spacings are 0.0030 atomic units.

alkali metals. While the positron surface states at the clean (100), (110), and (111) surfaces of Li are ''deep'' states, lying about 0.50 eV below the bulk bands, the other alkali-metal positron surface states fall barely below the corresponding bulk states (in the range 0.03–0.09 eV). These ''shallow'' states are a consequence of a more open structure of nuclei, permitting the positron surface-state wave function to penetrate much more effectively into the bulk region. This deeper penetration for more open structures results in the positron experiencing an average potential approaching that of the bulk. These distinctions between the open and more closely packed structures were not discovered in calculations that treated the bulk in the jellium approximation.[4]

The positronium work function with respect to the vacuum zero for the (100), (110), and (111) surfaces of Cu and alkali metals may be computed from the following relation:

$$\Phi_{\mathrm{Ps}}=\Phi_e+\Phi_p-E_B, \tag{5}$$

where the values of Φ_e are taken from Ref. 35, and $E_B=6.8$ eV is the positronium binding energy. The activation energies E_a required to thermally desorb positronium atoms from the (100), (110), and (111) surfaces of the alkali metals can be deduced from the Born-Haber cycle:

$$E_a=E_b+\Phi_e-E_B, \tag{6}$$

using the values for Φ_e from Ref. 35. The results for E_a and Φ_{Ps} are presented in Table II. As may be seen from Table II, the positronium activation energies for the (100), (110), and (111) surfaces of most alkali metals do not differ very much from the ones obtained for the transition-metal surface. This is due to the fact that the increase in the binding energy of the positron trapped at the alkali-metal surface is accompanied by a corresponding decrease of the bulk electron work function relative to its value for the transition metal. However, the predicted value of E_a for the (100) surface of Li is much smaller than the one found for Cu(100), Cu(110), and Cu(111) [$E_a\approx 0.04$ eV for Li(100), $E_a\approx 0.62$ eV for Cu(100), $E_a\approx 0.77$ eV for Cu(110), and $E_a\approx 0.98$ eV for Cu(111)], and in the cases of Na(100), Na(110), and Na(111), E_a exceeds their values for Cu(100), Cu(110), and Cu(111) by more than 1 eV. As Table II shows, Φ_{Ps} is predicted to be negative for Li(100), as in the case of transition-metal surfaces.[39,45] For all other alkali metals, Φ_{Ps} is found to be positive, although its value for Cs(100) is found to be relatively small ($\Phi_{\mathrm{Ps}}\approx 0.04$ eV).

The estimates for Φ_p, Φ_{Ps}, and E_a with respect to the vacuum level performed by other authors for Cu and alkali metals using different computational schemes are also presented in Table II. As Table II shows, estimates of the positronium work function obtained in this paper differ significantly for most alkali metals from the values obtained earlier

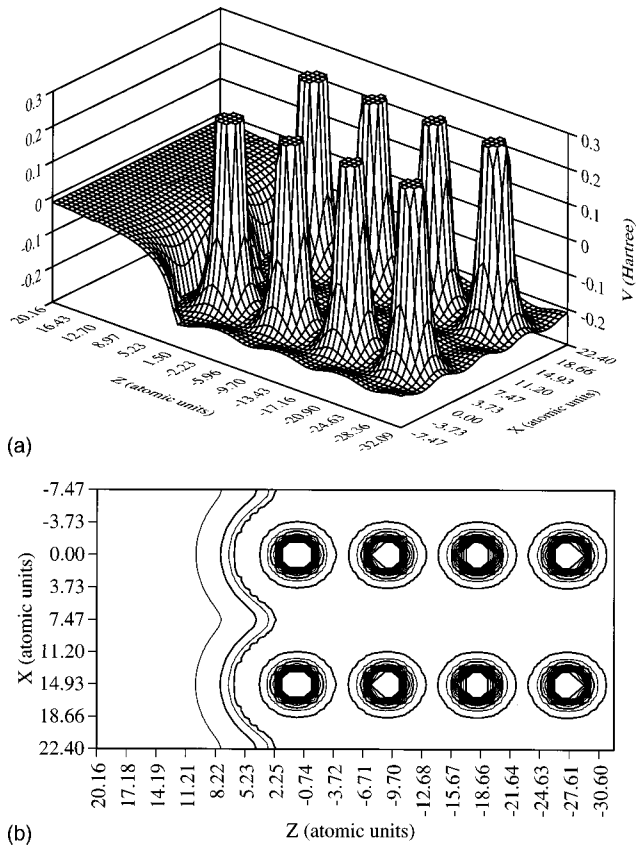

FIG. 11. Calculated potential for a positron trapped in a surface state at a clean (111) surface of Rb. Panel *A* shows 3D plot for $Y=0$ (view from the bulk). Panel *B* shows contour plot in the *X*-*Z* plane for $Y=0$. Vacuum is at the left in panel *B*. Contours are separated by 0.05 hartree.

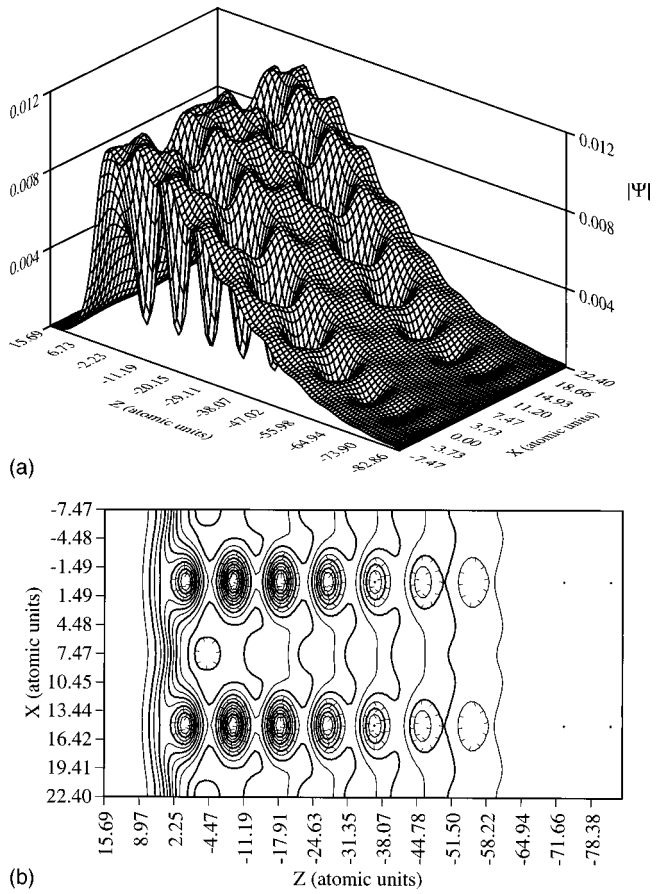

FIG. 12. Calculated ground-state wave function for a positron trapped in a surface state at a clean (111) surface of Rb. Panel *A* shows 3D plot for $Y=0$ (view from the bulk). Panel *B* shows contour plot in the *X*-*Z* plane for $Y=0$. Vacuum is at the left in panel *B*. Contour spacings are 0.0025 atomic units.

for Φ_{Ps} using other computational schemes.[39,43] In particular, Φ_{Ps} is found to be negative for Li(100), as in the case of transition-metal surfaces,[39,43] and in the case of Cs(100) the positronium work function is predicted to be relatively small ($\Phi_{Ps}=0.04$ eV) and it differs by ≈ 1 eV from the values obtained earlier. Differences between our values and those found by others previously are attributed to discrete lattice effects not included in earlier work and to the use of different computational schemes and potentials, while calculating different terms contributing to Φ_{Ps} in earlier studies.[39,43]

V. POSITRON ANNIHILATION CHARACTERISTICS

The total annihilation rate λ of the surface trapped positrons is calculated taking the electron-positron correlation effects explicitly into account by using the LDA. The expression for λ within LDA is given by the following equation:[38]

$$\lambda=\frac{\pi r_0^2 c}{e}\int d^3r\; n_+(\mathbf{r})n_-(\mathbf{r})\Gamma(n_-(\mathbf{r})), \tag{7}$$

where r_0 is the classical electron radius, c is the speed of light, $n_+(\mathbf{r})$ is the positron charge density, $n_-(\mathbf{r})$ is the electron density, and $\Gamma(n_-(\mathbf{r}))$ is the annihilation enhancement factor, which is related to the polarization of the electron gas of density $n_-(\mathbf{r})$ due to the presence of the positron. Since the electrons and the positively charged positrons are attracted to each other, the overlap of the positron and electron wave functions increases, leading to an increase of the positron annihilation rate. Outside the metal surface, the LDA must break down due to the fact that the positron correlation potential is no longer related to the electron density at the position of the positron, but is due to the presence of a metal surface with a large number of accumulated electrons on it. Following Ref. 46, we modify the LDA result for λ by assuming that the annihilation enhancement factor $\Gamma(n_-(\mathbf{r}))$ is zero for all $\mathbf{r}$ inside the image-potential region (the region of space where the positron correlation potential is given by the image potential), and is equal to the annihilation enhancement factor for a homogeneous electron gas, $\Gamma_{EG}(n_-(\mathbf{r}))$, elsewhere. The use of the electron gas approximation can be justified by the fact that most of the annihilations take place with valence electrons. According to recent many-body calculations,[37] the factor $\Gamma_{EG}(n_-(\mathbf{r}))$ may be represented by the following interpolation form:[47]

$$\Gamma_{EG}(n_-(\mathbf{r}))=1+1.23r_s+0.8295r_s^{3/2}-1.26r_s^2+0.3286r_s^{5/2}+r_s^3/6, \tag{8}$$

where $(4\pi/3)r_s^3 n_-=1$, with n_- the electron gas density and r_s the electron density parameter. This enhancement factor has been found to provide lifetimes in correspondence with experiments.[47]

TABLE II. Calculated values of positron work functions, Φ_p, positronium activation energies, E_a, and positronium work functions, Φ_{Ps}, at the clean (100), (110), and (111) surfaces of Li, Na, K, Rb, Cs, and Cu. Φ_p (HS) and Φ_{Ps} (HS) denote the results of Hodges and Stott for the positron and positronium work functions, respectively (Ref. 39). Φ_p (FFP) denotes theoretical results of Fletcher, Fry, and Pattnaik for the positron work functions (Ref. 41). Φ_p (NO) and Φ_{Ps} (NO) denote the results of Nieminen and Oliva for the positron and positronium work functions, respectively (Ref. 42). Φ_e denotes the experimental electron work functions (Refs. 49 and 50). $\Phi_p^{expt.}$ denotes the experimental positron work functions (Refs. 43 and 44).

Metal surface	Φ_p (eV)	$\Phi_p^{expt.}$ (eV)	Φ_p (HS) (eV)	Φ_p (NO) (eV)	Φ_p (FFP) (eV)	$\Phi_e^{expt.}$ (eV)	E_a (eV)	Φ_{Ps} (eV)	Φ_{Ps} (HS) (eV)	Φ_{Ps} (NO) (eV)
Cu(100)	−0.23	−0.3(2)		0.8[a]	0.9	4.59	0.62	−2.44	−3.13	−1.2[a]
Cu(110)	−0.14	−0.2(2)		0.8[a]	0.9	4.48	0.67	−2.46	−3.13	−1.2[a]
Cu(111)	−0.36	−0.4(1)		0.8[a]	0.9	4.85	0.85	−2.31	−3.13	−1.2[a]
Li(100)	3.44		4.35	5.2	6.1	2.93	0.06	−0.43	0.68	1.3
Li(110)	3.51		4.35	5.1	6.1	2.93	−0.04	−0.36	0.68	1.3
Li(111)	3.53		4.35	5.3	6.1	2.93	0.10	−0.34	0.68	1.3
Na(100)	5.85		4.62	4.5	6.1	2.70	1.80	1.75	0.54	0.4
Na(110)	5.88		4.62	4.2	6.1	2.70	1.81	1.78	0.54	0.4
Na(111)	5.88		4.62	4.8	6.1	2.70	1.80	1.78	0.54	0.4
K(100)	4.78		5.17	5.0	6.0[b]	2.30	0.33	0.28	0.82	0.5
K(110)	4.82		5.17	4.8	6.0[b]	2.30	0.36	0.32	0.82	0.5
K(111)	4.83		5.17	5.3	6.0[b]	2.30	0.35	0.33	0.82	0.5
Rb(100)	4.87		5.44	4.7	6.1	2.26	0.37	0.33	0.82	0.2
Rb(110)	4.82		5.44	4.4	6.1	2.26	0.33	0.28	0.82	0.2
Rb(111)	4.90		5.44	4.9	6.1	2.26	0.40	0.36	0.82	0.2
Cs(100)	4.89		5.71	4.9	6.1	2.14	0.26	0.20	1.09	0.95
Cs(110)	4.94		5.71	4.5	6.1	2.14	0.32	0.28	1.09	0.95
Cs(111)	4.93		5.71	5.2	6.1	2.14	0.29	0.27	1.09	0.95

[a]Reference 4.

[b]There is a typographical error in Table I of Ref. 41 for the Φ_p value for K. The correct Φ_p value for K has been taken from Fig. 1 of Ref. 41.

The positron annihilation rates $\lambda_{n,l}$ with the specific core-level electrons, described by n and l, are calculated from the overlap of positron and electron densities using the independent-particle model (IPM).[48] We expect the IPM,[48] which neglects electron-positron correlations, to provide a reasonable estimate of $\lambda_{n,l}$, since the core electrons are more tightly bound than valence electrons, and, therefore, the electron-positron correlations are relatively less important in calculations of the positron annihilation rate $\lambda_{n,l}$ with the specific core-level electrons than in calculations of the total annihilation rate λ. Within the IPM,[48] the annihilation rate $\lambda_{n,l}$ is given by the following expression:

$$\lambda_{n,l}=\pi r_0^2 c\int d^3r|\Psi_+(r)|^2\left(\sum_i |\Psi_{n,l}^i(r)|^2\right), \qquad (9)$$

where Ψ^+ is the positron wave function and $\Psi_{n,l}^i$ is the wave function of the core electron described by quantum numbers n and l. The summation is over all electron states in the atomic levels defined by quantum numbers n and l. The core annihilation probabilities $p_{n,l}$ with the specific core electron shells, described by quantum numbers n and l, can be obtained by dividing the partial positron annihilation rate $\lambda_{n,l}$ with the different core shells by the total positron annihilation rate λ: $p_{n,l}=\lambda_{n,l}/\lambda$. The computed values of the positron surface-state lifetimes, τ, and of the positron annihilation probabilities, $p_{n,l}$, with specific alkali-metal core-level electrons are presented in Tables III and IV.

VI. DISCUSSION

Since stability of positron surface states on the alkali metals depends upon computed energy differences that are very small for Na, K, Rb, and Cs (in the range 0.03–0.09 eV), we have studied carefully the reliability of these predictions. In obtaining these differences we used identical semi-infinite potentials for both the bulk and surface states, but with appropriate boundary conditions for the different states. Calculations were performed iteratively until energies converged to three significant figures. Thus the precision of the calculations was one order of magnitude greater than needed for accurate energy differences. The difference between bulk and surface states depends upon the form of potential used at the surface. As long as the vacuum level is unchanged, the bulk states are insensitive to changes in the details of the surface potentials, which only contribute terms of order $1/N$ to Φ_p, where N is the number of layers in the bulk. On the other hand, highly localized surface states can be strongly influenced by changes in the details of the surface potential. To investigate this possibility, we modified the only parameter in the surface potential, Z_0, to study its effect on surface-state stability. In the initial calculations, Z_0 was set equal to the Wigner-Seitz radius for each alkali metal. For test purposes it was then modified to the ionic radius, resulting in changes in Z_0 as large as 0.47 a.u. This modification made only very small changes in $\Delta E=E_b-\Phi_p$ for all the alkali metals except Li. This may be understood by examining the spatial dependence of the shallow surface states

TABLE III. Calculated values of positron lifetimes, τ, for the clean (100), (110), and (111) surfaces of Cu and alkali metals and for the bulk Cu and alkali metals. τ^{LDA} (ps) are theoretical positron bulk lifetimes obtained in Ref. 45 with the LMTO-ASA method using the LDA enhancement factor. $\tau(P)$ are theoretical results of Puska from Ref. 46. τ^{GGA} (ps) are theoretical positron bulk lifetimes obtained in Ref. 47 with the LMTO-ASA method using the density gradient correction scheme. $\tau_{\mathrm{expt.}}$ (ps) are experimental bulk results from Ref. 52.

System	τ (ps)	$\tau_{\mathrm{expt.}}$ (ps)	τ^{LDA} (ps)	$\tau(P)$ (ps)	τ^{GGA} (ps)
Cu(100)	478				
Cu(110)	474				
Cu(111)	502				
Bulk Cu	109	110	96	106	118
Li(100)	463				
Li(110)	448				
Li(111)	473				
Bulk Li	309	291(6)	257	305	282
Na(100)	352				
Na(110)	354				
Na(111)	352				
Bulk Na	347	338(7)	279	337	329
K(100)	419				
K(110)	395				
K(111)	407				
Bulk K	387	397(10)	329	387	392
Rb(100)	416				
Rb(110)	398				
Rb(111)	409				
Bulk Rb	393	406(10)	341	396	409
Cs(100)	423				
Cs(110)	410				
Cs(111)	417				
Bulk Cs	404	418(10)	356	407	430

which, like the bulk states, get a major portion of their total energy from sampling the bulk potential (e.g., Fig. 10). In all cases the predictions of stability were unchanged, so we are confident that, with this form of surface potential, there will always be stable surface states on each surface examined. Failure of earlier studies to find surface states on alkali metals[4] may be attributed to the fact that they are very shallow, and neglect of lattice structure and failure to use exactly the same reference level for bulk and surface potentials could easily miss them.[51,53]

The extent to which the positron surface-state wave function penetrates into the bulk can be understood qualitatively in terms of the energy difference between the surface and bulk states, ΔE, i.e., the larger the value of ΔE, the less the surface-state wave function penetrates into the bulk. This difference is relatively large for the (100), (110), and (111) surfaces of Li ($\Delta E \approx 0.37-0.44$ eV). In these cases, the positron surface-state wave function at the clean surface of Li is localized mostly on the vacuum side of the topmost layer of alkali-metal atoms. However, ΔE is found to be considerably smaller for the Li surfaces than for the cases of the (100), (110), and (111) surfaces of Cu, for which $\Delta E \approx 3.06-3.15$ eV. This explains the fact that the positron surface-bound-state wave function at the surface of Li penetrates further into the bulk than the one found for the surface of Cu.[27] It follows from the data presented in Table III that for the (100), (110), and (111) surfaces of Li, the calculated values for the positron surface-state lifetime, τ ($\tau \cong 463$, 448, and 473 ps, respectively) exceed considerably the value of τ for the bulk alkali metal ($\tau \cong 309$ ps), as expected. Though the positron surface-bound-state wave function at the (100), (110), and (111) surfaces of Li extends deeper into the metal lattice as compared to the one found for the (100), (110), and (111) surfaces of Cu, the computed positron surface-state lifetimes are found to be about the same [$\tau \cong 478$, 474, and 502 ps for the (100), (110), and (111) surfaces of Cu, respectively]. This is due to the smaller total electron density in the alkali metal as compared to the one in the transition metal.

As may be seen from Table III, the computed positron bulk lifetimes, τ, for alkali metals in this paper are found to be in good agreement with the experimental bulk values. This reflects the fact that the positron potential used in calculations provides a good approximation for the actual potential experienced by the positron in the bulk metal terminated by the (100), (110), and (111) surfaces.

The probabilities of the positron trapped at the (100), (110), and (111) surfaces of Li to annihilate with Li 1s electrons are computed to be 3.34%, 3.93%, and 4.41%, respectively, and are comparable with the sum of positron annihilation probabilities with Cu 3s and 3p core-level electrons at the clean (100), (110), and (111) surfaces, 3.86%, 3.64%, and 3.63%, respectively. [Both these positron annihilation probabilities contribute to the PAES $M_{2,3}VV$ signal intensity observed for the (100) surface of Cu.[26,27]] It may also be seen from Table IV that positron annihilation probabilities with the outer core-level electrons at the (100), (110), and (111) surfaces of other alkali metals are comparable with or larger than the sum of positron annihilation probabilities with Cu 3s and 3p core-level electrons at the clean surfaces of Cu, thus suggesting that the associated PAES signals can be observed from these surfaces of alkali metals.

The energy difference between the surface and bulk states is much smaller for the other alkali metals (of the order of 0.04–0.05 eV) and as a result the positron surface-state wave function extends much deeper into the metal lattice as compared to the cases of the (100), (110), and (111) surfaces of Li and Cu. This explains the fact that in the case of the other alkali metals, the positron surface-state lifetimes, while still larger than bulk positron lifetimes, are much closer to the bulk lifetimes than in the cases of the (100), (110), and (111) surfaces of Li and Cu [the differences in τ range from 5 ps for Na(100) and Na(111) to 22 ps for Rb(100)]. A similar trend is found in the values for positron annihilation probabilities with relevant core-level electrons computed for the clean (100), (110), and (111) surfaces of Na, K, Rb, and Cs and bulk alkali metals. It may be seen from Table IV that the sum of the probabilities of a positron trapped in a surface state at the clean (100), (110), and (111) surfaces of Cs to annihilate with Cs 4p and 4d core-level electrons is only a small fraction of the sum of the positron annihilation probabilities with Cu 3s and 3p core-level electrons for the clean (100) surface of Cu. As a consequence, the Cs $N_{4,5}VV$ PAES

TABLE IV. Calculated values of positron annihilation probabilities with relevant core-level electrons for the clean (100), (110), and (111) surfaces of Cu and alkali metals and for the bulk Cu and alkali metals.

System	Positron annihilation probabilities with core-level electrons (%)				
Level:	$2s$	$2p$	$3s$	$3p$	
Cu(100)	0.012	0.026	0.83	3.03	
Cu(110)	0.010	0.020	0.78	2.86	
Cu(111)	0.010	0.021	0.77	2.85	
Bulk Cu	0.021	0.045	1.47	5.29	
Level:	$1s$				
Li(100)	3.340				
Li(110)	3.930				
Li(111)	4.410				
Bulk Li	4.370				
Level:	$1s$	$2s$	$2p$		
Na(100)	0.220	3.170	4.150		
Na(110)	0.186	3.036	3.953		
Na(111)	0.220	3.140	4.000		
Bulk Na	0.192	3.212	4.202		
Level:	$1s$	$2s$	$2p$	$3s$	$3p$
K(100)	0.0002	0.021	0.054	1.052	4.365
K(110)	0.001	0.015	0.037	1.056	4.463
K(111)	0.001	0.017	0.044	1.073	4.485
Bulk K	0.0003	0.023	0.057	1.105	4.629
Level:	$3s$	$3s$	$3d$	$4s$	$4p$
Rb(100)	0.020	0.060	0.140	0.900	4.180
Rb(110)	0.014	0.047	0.117	0.876	4.214
Rb(111)	0.017	0.058	0.130	0.890	4.240
Bulk Rb	0.018	0.061	0.142	0.941	4.437
Level:	$4s$	$4p$	$4d$	$5s$	$5p$
Cs(100)	0.020	0.060	0.510	0.520	3.880
Cs(110)	0.013	0.052	0.480	0.480	3.800
Cs(111)	0.015	0.058	0.500	0.500	3.850
Bulk Cs	0.017	0.065	0.525	0.527	3.975

signals from the (100), (110), and (111) surfaces of Cs can be expected to be only a small fraction of the Cu $M_{2,3}VV$ PAES signals from the corresponding surfaces of Cu, thus requiring an intense positron beam to be measured within reasonable data accumulation times. This has been confirmed experimentally for one physical monolayer of Cs on the (100) surface of Cu at 173 K.[26]

Since the difference in the population of the positron bulk and surface states in alkali metals is small at high temperatures due to a small difference in the values of the positron bulk- and surface-bound-state energies, it might be difficult to distinguish the bulk and surface contributions to the positron-annihilation-induced Auger-electron signal. Lowering the temperature would decrease the rate of thermally activated positronium emission and increase the population of the positron surface state. This would improve the conditions for the observation and study of the PAES signal from alkali-metal surfaces due to the fact that the PAES intensity is directly proportional to the population of the positron surface-bound state.

VII. CONCLUSIONS

We have performed theoretical studies of positron states and annihilation characteristics at the clean surfaces of alkali metals. Positron surface states and positron work functions for the (100), (110), and (111) surfaces Li, Na, K, Rb, and Cs have been calculated from first principles using the modified superimposed-atom method, which takes into account discrete-lattice effects. In our calculations, the trapping of the positron, treated as a single charged particle in a ''correlation well'' in the proximity of surface atoms, has been described on the basis of a long-range image potential that has the same corrugations as the total electron density at a surface.

The positron surface and bulk state energies have been computed by solving the three-dimensional single-particle Schrödinger equation numerically using the finite difference relaxation technique. The same total electron density and the same potential have been used in the surface-state and bulk calculations. Stable positron surface states have been found in all cases, with the Li states lying about 0.5 eV below the bulk positron band, and other alkali metals having positron

surface states a few hundredths of an eV below the bulk bands.

It has been shown that in the case of the (100), (110), and (111) surfaces of Li, the positron is trapped mainly in the image-correlation well on the vacuum side of the topmost layer of alkali-metal atoms similar to the case of transition-metal surfaces. In the case of the other alkali-metal (Na, K, Rb, and Cs) surfaces, the positron surface-state wave functions extend considerably deeper into the metal lattice, having their maximum in the interstitial region between the topmost and the second layers of alkali-metal atoms.

It has been found that in the case of clean alkali-metal surfaces, the positron surface-state binding energies are considerably larger than in the case of clean transition-metal surfaces, reflecting the difference in the depth of the correlation well. The deeper well at the alkali metal's surface is a result in part of the lower total electron density in the alkali metal as compared to the transition metal, and to a change in the position of the image surface.

It has been shown that orientation-dependent variations of the atomic density and total electron density result in a corresponding dependence of the positron surface-state binding energy and positron work function, and that the largest values of the positron surface-state binding energy and positron work function are correlated with the planes of smallest atomic density.

The positronium activation energy and positronium work function for the clean surfaces of alkali metals have been computed as well.

The calculated positron surface and bulk state wave functions have been used to find the positron lifetimes and the positron annihilation probabilities with alkali-metal core-level electrons using the local-density approximation and the independent-particle model. The computed positron bulk lifetimes have been found to be in good agreement with experimental bulk values, and the positron lifetimes in the surface state have been found to be larger than in the bulk state, as expected. In the case of all alkali metals, positron annihilation probabilities with the outer core-level electrons at the (100), (110), and (111) surfaces have been found to be comparable to or larger than the sum of positron annihilation probabilities with Cu $3s$ and $3p$ core-level electrons at the clean surfaces of Cu. In the cases of Na, K, Rb, and Cs positron annihilation probabilities with more tightly-bound core-level electrons have been found to be low but comparable to the sum of positron annihilation probabilities with Cs $4p$ and $4d$ core-level electrons obtained for the (100) surface of Cu covered with one physical monolayer of Cs.

Though the difference in the population of the positron bulk and surface states in alkali metals is small at high temperatures due to a small difference in the values of the positron bulk- and surface-bound-state energies, lowering the temperature will improve the conditions for the observation and study of the PAES signal from clean alkali-metal surfaces. This is due to the fact that the PAES intensity is directly proportional to the population of the positron surface-bound state, and lowering the temperature would decrease the rate of thermally activated positronium emission and increase the population of the positron surface state.

ACKNOWLEDGMENTS

We would like to thank A. P. Mills, Jr., R. M. Nieminen, K. G. Lynn, R. N. West, and F. M. Jacobsen for useful and stimulating discussions. This work was supported in part by the National Science Foundation (DMR 9502459) and the Robert A. Welch Foundation.

*Permanent address: Department of Physics, Kazan State University, Kazan 420008, Russia.

[1] M. W. Cole and M. H. Cohen, Phys. Rev. Lett. **23**, 1238 (1969); M. W. Cole, Phys. Rev. B **2**, 4239 (1970).
[2] J. Sak, Phys. Rev. B **6**, 3981 (1972); E. Evans and D. L. Mills, *ibid.* **8**, 4004 (1973).
[3] C. H. Hodges and M. J. Stott, Solid State Commun. **12**, 1153 (1973).
[4] R. M. Nieminen and C. H. Hodges, Phys. Rev. B **18**, 2568 (1978).
[5] N. Barberan and P. M. Echenique, Phys. Rev. B **19**, 5431 (1979).
[6] M. Barbiker, Physica B&C **103**, 289 (1981).
[7] G. Barton, J. Phys. C **14**, 3975 (1981).
[8] R. M. Nieminen and M. J. Puska, Phys. Rev. Lett. **50**, 281 (1983).
[9] R. M. Nieminen and Kjeld O. Jensen, Phys. Rev. B **38**, 5764 (1988).
[10] Kjeld O. Jensen and A. Weiss, Phys. Rev. B **41**, 3928 (1990).
[11] Kjeld O. Jensen and A. B. Walker, J. Phys. F **18**, L277 (1988).
[12] G. Barton, J. Phys. C **15**, 4727 (1982); C. Cuthbert, *ibid.* **18**, 4561 (1985).
[13] P. M. Platzman and N. Tzoar, Phys. Rev. B **33**, 5900 (1986).
[14] A. P. Mills, Jr., Solid State Commun. **31**, 623 (1979).
[15] K. G. Lynn, Phys. Rev. Lett. **43**, 391 (1979).
[16] K. G. Lynn and D. O. Welch, Phys. Rev. B **22**, 99 (1980); K. G. Lynn and H. Lutz, *ibid.* **22**, 4143 (1980).
[17] I. J. Rosenberg, A. H. Weiss, and K. F. Canter, J. Vac. Sci. Technol. **17**, 253 (1980).
[18] Alex Weiss, R. Mayer, M. Jibaly, C. Lei, D. Mehl, and K. G. Lynn, Phys. Rev. Lett. **61**, 2245 (1988).
[19] A. R. Koymen, K. H. Lee, D. Mehl, Alex Weiss, and K. O. Jensen, Phys. Rev. Lett. **68**, 2378 (1992).
[20] N. G. Fazleev, J. L. Fry, J. H. Kaiser, A. R. Koymen, K. H. Lee, T. D. Niedzwiecki, and A. Weiss, Phys. Rev. B **49**, 10 577 (1994).
[21] D. Mehl, A. R. Koymen, Kjeld O. Jensen, Fred Gotwald, and Alex Weiss, Phys. Rev. B **41**, 799 (1990).
[22] R. Mayer, A. Schwab, and A. Weiss, Phys. Rev. B **42**, 1881 (1990).
[23] K. H. Lee, A. R. Koymen, D. Mehl, K. O. Jensen, and A. Weiss, Surf. Sci. **264**, 127 (1992).
[24] A. R. Koymen, K. H. Lee, G. Yang, K. O. Jensen, and A. H. Weiss, Phys. Rev. B **48**, 2020 (1993).
[25] A. Weiss, Mater. Sci. Forum **105–110**, 511 (1992); Solid State Phenom. **28&29**, 317 (1992/1993).
[26] N. G. Fazleev, J. L. Fry, K. Kuttler, A. R. Koymen, and A. H. Weiss, Appl. Surf. Sci. **85**, 26 (1995).
[27] N. G. Fazleev, J. L. Fry, K. Kuttler, A. R. Koymen, and A. H. Weiss, Phys. Rev. B **52**, 5351 (1995).
[28] N. G. Fazleev, J. L. Fry, K. Kuttler, A. R. Koymen, and A. H. Weiss, Mater. Sci. Forum **175-178**, 153 (1995).
[29] N. G. Fazleev, J. L. Fry, J. H. Kaiser, A. R. Koymen, T. D. Niedzwiecki, and Alex Weiss, in *Positron Beams for Solids and Surfaces*, edited by E. Ottewitte and A. Weiss, AIP Conf. Proc.

No. 303 (AIP, New York, 1994), p. 208
[30] G. E. Kimball and G. H. Shortley, Phys. Rev. **45**, 815 (1934).
[31] O. Gunnarsson and B. I. Lundqvist, Phys. Rev. B **13**, 4274 (1976).
[32] D. M. Ceperly and B. J. Adler, Phys. Rev. Lett. **45**, 566 (1980).
[33] F. Herman and S. Skillman, *Atomic Structure Calculations* (Englewood Cliffs, Prentice-Hall, NJ, 1963).
[34] M. Weinert and R. E. Watson, Phys. Rev. B **29**, 3001 (1984).
[35] J. Holtz and F. K. Schulte, in *Springer Tracts in Modern Physics* (Springer, Heidelberg, 1979), Vol. 85.
[36] N. W. Ashcroft and N. D. Mermin, *Solid State Physics* (Holt, Rinehart, and Winston, New York, 1976).
[37] J. Arponen and E. Pajanne, Ann. Phys. (N.Y.) **121**, 343 (1979).
[38] E. Boronski and R. M. Nieminen, Phys. Rev. B **34**, 3820 (1986).
[39] C. H. Hodges and M. J. Stott, Phys. Rev. B **7**, 73 (1973).
[40] J. L. Fry and P. C. Pattnaik, in *Positron Annihilation*, edited by P. G. Coleman, S. C. Sharma, and L. M. Diana (North-Holland, Amsterdam, 1982), p. 159.
[41] G. Fletcher, J. L. Fry, and P. C. Pattnaik, Phys. Rev. B **27**, 3987 (1983).
[42] R. M. Nieminen and J. Oliva, Phys. Rev. B **22**, 2226 (1980).
[43] M. Jibaly, E. C. Kellogg, A. Weiss, A. R. Koymen, D. Mehl, and L. Stiborek, Mater. Sci. Forum **105-110**, 1399 (1992).
[44] D. A. Fisher, K. L. Lynn, and W. E. Frieze, Phys. Rev. B **33**, 4479 (1986).
[45] R. M. Nieminen and C. H. Hodges, Solid State Commun. **18**, 1115 (1976).
[46] R. M. Nieminen, M. J. Puska, and M. Manninen, Phys. Rev. Lett. **53**, 1298 (1984).
[47] K. O. Jensen, J. Phys.: Condens. Matter **1**, 10 595 (1989).
[48] E. Bonderup, J. U. Andersen, and D. N. Lowy, Phys. Rev. B **20**, 883 (1979).
[49] M. J. Puska, J. Phys.: Condens. Matter **3**, 3455 (1991).
[50] B. Barbiellini, M. J. Puska, T. Lorhonen, A. Harju, T. Torsti, and R. M. Nieminen, Phys. Rev. B **54**, 2397 (1996).
[51] A. Seeger, F. Barnhart, and W. Bauer, in *Positron Annihilation*, edited by L. Dorikens-Vanpraet, M. Dorikens, and D. Segers (World Scientific, Singapore, 1989), p. 275.
[52] A. P. Mills, Jr., in *The Proceedings of the International School of Physics ''Enrico Fermi,'' 1981*, edited by W. Brandt (North-Holland, Amsterdam, 1983), p. 432.
[53] H. Weisberg and S. Berko, Phys. Rev. **154**, 249 (1967); I. K. Mackenzie, in *The Proceedings of the International School of Physics ''Enrico Fermi''* (Ref. 52), p. 200; R. N. West, *Positron Studies of Condensed Matter* (Taylor & Francis, London, 1974).